Energy Storage Materials xx (xxxx) xxxx–xxxx

Contents lists available at ScienceDirect

Energy Storage Materials

journal homepage: www.elsevier.com/locate/ensm

Cobalt induced multi-plateau behavior in TiNi-based Ni-MH electrodes

Hoda Emami, Fermin Cuevas*

Université Paris Est, ICMPE (UMR7182), CNRS, UPEC, F-94320 Thiais, France

ARTICLE INFO

Keywords:
Metal hydrides
Intermetallics
TiNi
TiCo
Ni-MH batteries

ABSTRACT

Nickel-metal hydride batteries Ni-*M*H with higher energy densities are requested while keeping good capacity retention on cycling. In this context, the structural, solid-gas and electrochemical hydrogenation properties of $TiNi_{1-x}Co_x$ ($0 \le x \le 0.5$) compounds have been investigated. Metallurgical characterizations evidence the formation of Ti(Ni,Co) pseudobinary compounds crystallizing in the cubic CsCl-type structure with lattice parameter decreasing with Co-content. Co-substitution induces a multi-plateau behavior in both solid-gas and electrochemical isotherms even at the lowest Co-content here studied ($x \le 0.1$). Moreover, this substitution reduces the thermodynamic stability of Ti(Ni,Co) hydrides though it has little influence on discharge capacities, which are limited to 150 mAh/g at C/10 regime. Excellent capacity retention for 30 cycles is observed for low Co-contents ($x \le 0.3$). The Co-induced multi-plateau behavior and the good capacity retention demonstrate the interest of using Co-metal as additive in TiNi-based Ni-*M*H electrodes for improving their cycle-life.

1. Introduction

In the last years, performances of Li-ion batteries have surpassed nickel-metal hydride (Ni-*M*H) ones in terms of energy density and self-discharge properties. Nevertheless, the latter are still preferred for specific applications, such as portable power tools and hybrid electric vehicles, thanks to their robustness, lower price and safety [1,2]. The active material of the negative electrode of Ni-*M*H batteries is an AB_n intermetallic compound that reversibly reacts with hydrogen from the aqueous alkaline electrolyte [3–5]. Here, *A* stands for an early transition or rare-earth metal, while *B* is a last transition metal. The *A* metals have the property of forming highly stable hydrides, whereas the *B* ones form unstable ones. Today, AB_5 and AB_3 compounds with typical discharge capacities of 320 and 380 mAh/g, respectively, are used in commercial Ni-*M*H batteries. Their main drawback is that all of them contain scarce rare-earths and their mass capacity is limited by their high molecular weight. As an alternative, AB_2 and *AB* intermetallics are foreseen as promising electrode materials for the next generation of Ni-*M*H batteries.

Light-weight Ti-based *AB* intermetallics such as TiFe, TiCo and TiNi have been considered since long time as hydrogen storage materials. TiFe is particularly interesting since it forms $TiFeH_2$ dihydride close to normal conditions of pressure and temperature. Unfortunately, TiFe suffers from surface passivation in alkaline media leading to low electrochemical activity [6]. In contrast, TiNi which forms at normal conditions a hydride with lower hydrogen content, $TiNiH_{1.4}$, exhibits good resistance to corrosion and high electrocatalytic activity [7,8]. By electrochemical cycling, TiNi typically exhibits a reversible capacity of 150 mAh/g at C/10 regime, which only represents 40% of its total hydrogen content [9]. In-situ neutron diffraction measurements have demonstrated that such a limited reversible capacity is exclusively provided by hydrogen solubility in the β-hydride phase (from TiNiH to $TiNiH_{1.4}$) [10]. Recovery of the full storage capacity of TiNi (350 mAh/g for 1.4 hydrogen atoms per formula unit) is expected to be attained if TiNiH hydride is destabilized by suitable chemical substitutions.

We have explored the effect of chemical substitutions on the solid-gas and electrochemical properties of TiNi. In particular, the substitution of Ti by Zr on the crystallographic *A*-site [11–13], and that of Ni by Pd [14,15] or Cu [10] on the *B*-site have been considered. These studies have shown that TiNi-based compounds experimentally provide discharge capacities as high as 370 mAh/g and may potentially reach 600 mAh/g for $Ti_{0.88}Zr_{0.12}NiH_{2.6}$ hydride if all hydrogen atoms could be electrochemically discharged. However, a compromise between high reversible capacity and extended cycle-life is observed so far. This results from severe alloy decrepitation due to large mechanical strains associated to the large difference between the unit-cell volume of metal and hydride phases. Same issue was recognized in the early stage of research in $LaNi_5$-type electrodes and it was successfully solved by the partial substitution of Ni by Co atoms [16,17]. This substitution promotes the formation of intermediate hydride phases, which existence was proved by crystallographic studies and revealed by the multi-plateau behavior of $La(Ni,Co)_5$ hydrogen isotherms [18,19].

In this work, we investigate the effect of nickel by cobalt substitu-

* Corresponding author.
E-mail address: cuevas@icmpe.cnrs.fr (F. Cuevas).

http://dx.doi.org/10.1016/j.ensm.2016.11.008
Received 26 September 2016; Received in revised form 17 November 2016; Accepted 19 November 2016
Available online xxxx

tion on the structural and hydrogenation properties of TiNi. Our aim is to determine whether intermediate hydride phases are also found in the Ti(Ni,Co)-H system and if their existence have beneficial effects on its use as negative electrodes of Ni-*M*H battery.

2. Experimental methods

Six $Ti_{1.01}Ni_{0.99-x}Co_x$ intermetallic compounds with nominal composition of x=0, 0.1, 0.2, 0.3, 0.4 and 0.5 were synthesized by induction melting in the form of alloy ingots. To ensure chemical homogeneity, the ingots were melted four times and then annealed at 1173 K for 4 weeks. Their chemical composition and microstructure were investigated by Electron Probe Micro Analysis (EPMA) with a Cameca SX-100 device. Metallurgical characterization as concerns martensitic transformation temperatures were determined by Differential Scanning Calorimetry (DSC) using a TA Q100 calorimeter in the range 200–400 K at the heating/cooling rate of 10 K/min. Samples were sealed in aluminum pans for this purpose. The crystal structure of these compounds and their hydrides was characterized at room temperature (RT) by powder X-ray diffraction (XRD) with a θ-θ Bragg-Brentano D8-Bruker diffractometer using CuK_α radiation. The intermertallics are too tough to be obtained in powder form by mechanical crushing. To circumvent this issue, they were first embrittled by hydrogenation, next manually crushed to powder and then thermally desorbed by heating at 873 K under secondary vacuum.

Hydrogenation thermodynamics were characterized by monitoring Pressure Composition Temperature (PCT) isotherms using the Sievert's method in home-made manometric benches. Absorption and desorption isotherms were measured at 423 K in the pressure range P_{H2} from 10^{-4} to 1 MPa. Samples were activated for three absorption/desorption cycles before PCT acquisition. Absorption was carried out at P_{H2}=3 MPa, T=423 K and desorption at T=773 K under primary vacuum.

Electrochemical properties were determined by galvanostatic cycling at RT in one-compartment cell. Negative working electrodes with typical mass 300 mg were made of Ti(Ni,Co) powders sieved under 63 µm and mixed with conductive black carbon and PTFE in 90:5:5 weight ratio. This mixture was spread out in 250 µm thick sheets and compressed onto a Ni current collector. A positive $NiOOH/Ni(OH)_2$ electrode was used as the counter electrode and the potential was measured versus a Hg/HgO reference electrode (Hg/HgO vs. SHE=0.098 V). A poly-amide sheet was placed between the positive and negative electrode as a separator to avoid electrical shortcut. 6 M KOH aqueous solution was used as electrolyte both in the electrochemical cell and in the reference electrode to avoid OH^- concentration gradients. The galvanostatic cycling was performed at the rate of C/10 (full capacity C in 10 hours) with a cutoff potential of −0.7 V vs. Hg/HgO. Electrochemical isotherms were obtained at RT by the Galvanostatic Intermittent Titration Technique (GITT) after electrode activation for three cycles. All electrochemical experiments were computer monitored using a VMP3 galvanostat from Biologic.

3. Results and discussion

3.1. Metallurgical characterization

The microstructure and chemical composition of phases in $Ti_{1.01}Ni_{0.99-x}Co_x$ ingots were analyzed by EPMA. Micrographs taken in back-scattered electron mode (Fig S1 in Supplementary material) show tiny precipitates (< 5% in volume) distributed along grain boundaries of a main matrix phase. Chemical analysis of both phases is gathered in Table 1. It indicates that the main phase is *AB*-type Ti(Ni,Co), whereas the precipitates are A_2B-type $Ti_2(Ni,Co)$. Formation of $Ti_2(Ni,Co)$ secondary phase in Ti-rich *AB*-compounds is in agreement with the ternary Ti-Ni-Co phase diagram [20]. For all compounds, the chemical composition of the main phase is in close agreement to the nominal composition. For each alloy composition, the Ni/Co atomic ratio is roughly the same in the main and the secondary phase.

Table 1
Nominal and EPMA chemical composition of $Ti_{1.01}Ni_{0.99-x}Co_x$ alloy ingots. Standard deviations referred to the last digit are given in parenthesis.

x	Nominal composition	Main phase (EPMA)	Secondary phase (EPMA)
0	$Ti_{1.01}Ni_{0.99}$	$Ti_{1.01(1)}Ni_{0.95(7)}$	$Ti_{1.80(1)}Ni_{1.19(2)}$
0.1	$Ti_{1.01}Ni_{0.89}Co_{0.1}$	$Ti_{1.01(2)}Ni_{0.88(1)}Co_{0.11(2)}$	$Ti_{1.99(1)}Ni_{0.91(1)}Co_{0.09(4)}$
0.2	$Ti_{1.01}Ni_{0.79}Co_{0.2}$	$Ti_{1.00(2)}Ni_{0.78(2)}Co_{0.22(2)}$	$Ti_{1.89(5)}Ni_{0.82(1)}Co_{0.18(5)}$
0.3	$Ti_{1.01}Ni_{0.69}Co_{0.3}$	$Ti_{1.01(1)}Ni_{0.68(6)}Co_{0.31(1)}$	$Ti_{1.96(2)}Ni_{0.75(1)}Co_{0.28(6)}$
0.4	$Ti_{1.01}Ni_{0.59}Co_{0.4}$	$Ti_{1.01(3)}Ni_{0.56(2)}Co_{0.43(3)}$	$Ti_{1.95(6)}Ni_{0.68(2)}Co_{0.37(2)}$
0.5	$Ti_{1.01}Ni_{0.49}Co_{0.5}$	$Ti_{1.00(2)}Ni_{0.47(2)}Co_{0.53(3)}$	$Ti_{1.96(1)}Ni_{0.58(1)}Co_{0.46(1)}$

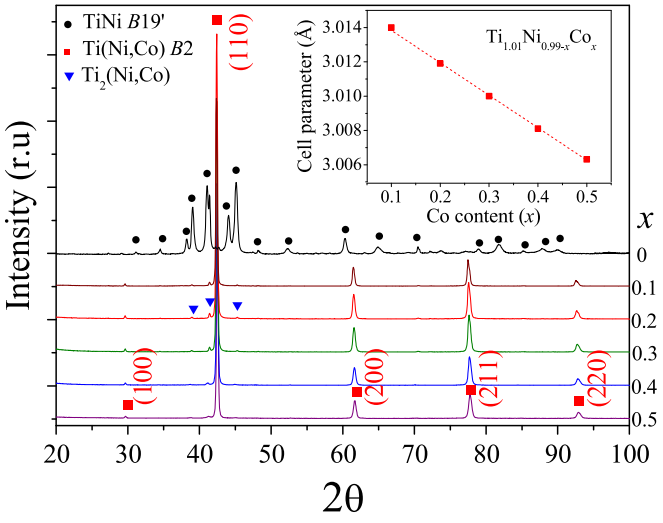

Fig. 1. XRD patterns of $Ti_{1.01}Ni_{0.99-x}Co_x$ ($0 \le x \le 0.5$) compounds at RT. Diffraction peaks for the binary TiNi compound (marked by black circles) are assigned to the monoclinic *B*19′ structure. Diffraction peaks for the pseudo-binary Ti(Ni,Co) compounds (marked by red squares) are indexed in the cubic *B*2 structure (S.G. $Pm\bar{3}m$). Diffraction peaks of the secondary $Ti_2(Ni,Co)$ phase are marked by blue triangles. (For interpretation of the references to color in this figure legend, the reader is referred to the web version of this article.)

The crystal structure of $Ti_{1.01}Ni_{0.99-x}Co_x$ compounds in powder form has been analyzed by XRD at RT. The XRD patterns are shown in Fig. 1. Except for the binary TiNi compound, all diffraction patterns can be indexed in the cubic *B*2 structure (Strukturbericht designation, CsCl-type, space group S.G. $Pm\bar{3}m$) with minor contribution of $Ti_2(Ni,Co)$ secondary phases (S.G.: $Fd\bar{3}m$, a≈11.3 Å). As shown in the inset of Fig. 1, the cell parameter of the cubic *B*2 structure linearly decreases with Co content. This relationship follows the Vegard's law, which usually applies to pseudo-binary compounds, since the lattice parameter of TiCo (2.995 Å) is shorter than that of TiNi (3.015 Å) crystallizing in the CsCl-type structure [21]. It can be noted, however, that in the present investigation the Co-free compound crystallizes at RT in the monoclinic *B*19' structure (S.G. $P2_1/m$), a fact that is characteristic of Ti-rich TiNi compounds [22].

For a better understanding of the crystallographic results and to get a full metallurgical characterization of $Ti_{1.01}Ni_{0.99-x}Co_x$ compounds, their thermal stability close to room temperature was studied by DSC. Structural changes near room temperature are a typical feature of TiNi-based alloys and are at the basis of their shape memory properties [22]. They concern martensitic transformations that are accompanied by significant heat exchange. Therefore, structural changes can be detected and by DSC analysis, which also allows for determination of phase transformation temperatures. The DSC runs for all studied compounds are displayed in Fig. S2 in Supplementary material. As a